

# First Measurement of $\pi^- e \rightarrow \pi^- e\gamma$ Pion Virtual Compton Scattering

March 2, 2019

The SELEX Collaboration

A. Ocherashvili<sup>*l,14*</sup>, G. Alkhazov<sup>*k*</sup>, A.G. Atamantchouk<sup>*k,1*</sup>, M.Y. Balatz<sup>*h,1*</sup>,  
 N.F. Bondar<sup>*k*</sup>, P.S. Cooper<sup>*e*</sup>, L.J. Dauwe<sup>*q*</sup>, G.V. Davidenko<sup>*h*</sup>, U. Dersch<sup>*i,2*</sup>,  
 A.G. Dolgolenko<sup>*h*</sup>, G.B. Dzyubenko<sup>*h*</sup>, R. Edelstein<sup>*c*</sup>, L. Emediato<sup>*s*</sup>,  
 A.M.F. Endler<sup>*d*</sup>, J. Engelfried<sup>*m,e*</sup>, I. Eschrich<sup>*i,3*</sup>, C.O. Escobar<sup>*s,4*</sup>,  
 A.V. Evdokimov<sup>*h*</sup>, I.S. Filimonov<sup>*j,1*</sup>, F.G. Garcia<sup>*s,e*</sup>, M. Gaspero<sup>*r*</sup>, I. Giller<sup>*l*</sup>,  
 V.L. Golovtsov<sup>*k*</sup>, P. Gouffon<sup>*s*</sup>, E. GÜlmez<sup>*b*</sup>, He Kangling<sup>*g*</sup>, M. Iori<sup>*r*</sup>, S.Y. Jun<sup>*c*</sup>,  
 M. Kaya<sup>*p*</sup>, J. Kilmer<sup>*e*</sup>, V.T. Kim<sup>*k*</sup>, L.M. Kochenda<sup>*k*</sup>, I. Konorov<sup>*i,5*</sup>,  
 A.P. Kozhevnikov<sup>*f*</sup>, A.G. Krivshich<sup>*k*</sup>, H. Krüger<sup>*i,6*</sup>, M.A. Kubantsev<sup>*h*</sup>,  
 V.P. Kubarovskiy<sup>*f*</sup>, A.I. Kulyavtsev<sup>*c,7*</sup>, N.P. Kuropatkin<sup>*k*</sup>, V.F. Kurshetsov<sup>*f*</sup>,  
 A. Kushnirenko<sup>*c*</sup>, S. Kwan<sup>*e*</sup>, J. Lach<sup>*e*</sup>, A. Lamberto<sup>*t*</sup>, L.G. Landsberg<sup>*f*</sup>, I. Larin<sup>*h*</sup>,  
 E.M. Leikin<sup>*j*</sup>, Li Yunshan<sup>*g*</sup>, M. Luksys<sup>*n*</sup>, T. Lungov<sup>*s,8*</sup>, V.P. Maleev<sup>*k*</sup>, D. Mao<sup>*c,7*</sup>,  
 Mao Chensheng<sup>*g*</sup>, Mao Zhenlin<sup>*g*</sup>, P. Mathew<sup>*c,9*</sup>, M. Mattson<sup>*c*</sup>, V. Matveev<sup>*h*</sup>,  
 E. McCliment<sup>*p*</sup>, M.A. Moinester<sup>*l*</sup>, V.V. Molchanov<sup>*f*</sup>, A. Morelos<sup>*m*</sup>,  
 K.D. Nelson<sup>*p,10*</sup>, A.V. Nemitzkin<sup>*j*</sup>, P.V. Neoustroev<sup>*k*</sup>, C. Newsom<sup>*p*</sup>, A.P. Nilov<sup>*h*</sup>,  
 S.B. Nurushev<sup>*f*</sup>, Y. Onel<sup>*p*</sup>, E. Ozel<sup>*p*</sup>, S. Ozkorucuklu<sup>*p*</sup>, A. Penzo<sup>*t*</sup>, S.V. Petrenko<sup>*f*</sup>,  
 P. Pogodin<sup>*p*</sup>, M. Procario<sup>*c,11*</sup>, V.A. Prutskoi<sup>*h*</sup>, E. Ramberg<sup>*e*</sup>, G.F. Rappazzo<sup>*t*</sup>,  
 B.V. Razmyslovich<sup>*k*</sup>, V.I. Rud<sup>*j*</sup>, J. Russ<sup>*c*</sup>, P. Schiavon<sup>*t*</sup>, J. Simon<sup>*i,12*</sup>,  
 A.I. Sitnikov<sup>*h*</sup>, D. Skow<sup>*e*</sup>, V.J. Smith<sup>*o*</sup>, M. Srivastava<sup>*s*</sup>, V. Steiner<sup>*l*</sup>, V. Stepanov<sup>*k*</sup>,  
 L. Stutte<sup>*e*</sup>, M. Svoiski<sup>*k*</sup>, N.K. Terentyev<sup>*k,c*</sup>, G.P. Thomas<sup>*a*</sup>, L.N. Uvarov<sup>*k*</sup>,  
 A.N. Vasiliev<sup>*f*</sup>, D.V. Vavilov<sup>*f*</sup>, V.S. Verebryusov<sup>*h*</sup>, V.A. Victorov<sup>*f*</sup>,  
 V.E. Vishnyakov<sup>*h*</sup>, A.A. Vorobyov<sup>*k*</sup>, K. Vorwalter<sup>*i,13*</sup>, J. You<sup>*c,e*</sup>, Zhao Wenheng<sup>*g*</sup>,  
 Zheng Shuchen<sup>*g*</sup>, R. Zukarnovich-Funchal<sup>*s*</sup>

<sup>*a*</sup>Ball State University, Muncie, IN 47306, U.S.A.

<sup>*b*</sup>Bogazici University, Bebek 80815 Istanbul, Turkey

<sup>*c*</sup>Carnegie-Mellon University, Pittsburgh, PA 15213, U.S.A.

<sup>*d*</sup>Centro Brasileiro de Pesquisas Físicas, Rio de Janeiro, Brazil

<sup>*e*</sup>Fermilab, Batavia, IL 60510, U.S.A.

<sup>f</sup>Institute for High Energy Physics, Protvino, Russia

<sup>g</sup>Institute of High Energy Physics, Beijing, P.R. China

<sup>h</sup>Institute of Theoretical and Experimental Physics, Moscow, Russia

<sup>i</sup>Max-Planck-Institut für Kernphysik, 69117 Heidelberg, Germany

<sup>j</sup>Moscow State University, Moscow, Russia

<sup>k</sup>Petersburg Nuclear Physics Institute, St. Petersburg, Russia

<sup>l</sup>Tel Aviv University, 69978 Ramat Aviv, Israel

<sup>m</sup>Universidad Autónoma de San Luis Potosí, San Luis Potosí, Mexico

<sup>n</sup>Universidade Federal da Paraíba, Paraíba, Brazil

<sup>o</sup>University of Bristol, Bristol BS8 1TL, United Kingdom

<sup>p</sup>University of Iowa, Iowa City, IA 52242, U.S.A.

<sup>q</sup>University of Michigan-Flint, Flint, MI 48502, U.S.A.

<sup>r</sup>University of Rome “La Sapienza” and INFN, Rome, Italy

<sup>s</sup>University of São Paulo, São Paulo, Brazil

<sup>t</sup>University of Trieste and INFN, Trieste, Italy

## Abstract

Pion Virtual Compton Scattering (VCS) via the reaction  $\pi^- e \rightarrow \pi^- e\gamma$  was observed in the Fermilab E781 SELEX experiment. SELEX used a 600 GeV/c  $\pi^-$  beam incident on target atomic electrons, detecting the incident  $\pi^-$  and the final state  $\pi^-$ , electron and  $\gamma$ . Theoretical predictions based on chiral perturbation theory are incorporated into a Monte Carlo simulation of the experiment and are compared to the data. The number of reconstructed events (9) and their distribution with respect to the kinematic variables (for the kinematic region studied) are in reasonable accord with the predictions. The corresponding  $\pi^-$  VCS experimental cross section is  $\sigma = 38.8 \pm 13$  nb, in agreement with the theoretical expectation  $\sigma = 34.7$  nb.

---

<sup>1</sup>deceased

<sup>2</sup>Present address: Infion, München, Germany

<sup>3</sup>Now at Imperial College, London SW7 2BZ, U.K.

<sup>4</sup>Now at Instituto de Física da Universidade Estadual de Campinas, UNICAMP, SP, Brazil

<sup>5</sup>Now at Physik-Department, Technische Universität München, 85748 Garching, Germany

<sup>6</sup>Present address: The Boston Consulting Group, München, Germany

<sup>7</sup>Present address: Lucent Technologies, Naperville, IL

<sup>8</sup>Now at Instituto de Física Teórica da Universidade Estadual Paulista, São Paulo, Brazil

<sup>9</sup>Present address: SPSS Inc., Chicago, IL

<sup>10</sup>Now at University of Alabama at Birmingham, Birmingham, AL 35294

<sup>11</sup>Present address: DOE, Germantown, MD

<sup>12</sup>Present address: Siemens Medizintechnik, Erlangen, Germany

<sup>13</sup>Present address: Deutsche Bank AG, Eschborn, Germany

<sup>14</sup>Present address: Imadent Ltd., Rehovot 76702, Israel

# 1 Introduction

The electric ( $\bar{\alpha}$ ) and magnetic ( $\bar{\beta}$ ) pion polarizabilities characterize the pion's deformation in an electromagnetic field, as occurs during  $\gamma\pi$  Compton scattering. They depend on the rigidity of the pion's internal structure as a composite particle, and are therefore important dynamical quantities to test the validity of theoretical models. Based on QCD chiral dynamics, the chiral perturbation theory effective Lagrangian, using data from radiative pion beta decay, predicts the pion electric and magnetic polarizabilities  $\bar{\alpha}_\pi = -\bar{\beta}_\pi = 2.7 \pm 0.4$ , expressed in units of  $10^{-43} \text{ cm}^3$  [1, 2, 3]. Other theoretical predictions are also available [1].

The pion polarizabilities are usually investigated via their effect on the shape of the measured  $\gamma\pi \rightarrow \gamma\pi$  Real Compton Scattering (RCS) angular distribution, as in Ref. [4]. Since pion targets are unavailable, pion RCS is approximated using different artifices, as shown in Fig. 1: the  $\pi^-Z \rightarrow \pi^-Z\gamma$  Primakoff [5] and  $\gamma p \rightarrow \gamma\pi^+n$  radiative pion photoproduction reactions [6]; or by the crossing symmetry  $\gamma\gamma \rightarrow \pi^+\pi^-$  two-photon reaction [2, 7]. In the Primakoff scattering, a high energy pion scatters from a (virtual, practically real) photon in the Coulomb field of the target nucleus. Values of  $\bar{\alpha}$  measured by these experiments are given in Table 1.

Reaction	$\bar{\alpha} [10^{-43} \text{ cm}^3]$	Reference
$\pi^-Z \rightarrow \pi^-Z\gamma$	$6.8 \pm 1.4 \pm 1.2$	[5]
$\gamma p \rightarrow \gamma\pi^+n$	$20 \pm 12$	[6]
$\gamma\gamma \rightarrow \pi^+\pi^-$	$2.2 \pm 1.6$	[2, 7]

Table 1: Experimental values of  $\bar{\alpha}$ .

They cover a large range of values and have large uncertainties. New high precision pion polarizability measurements are therefore needed.

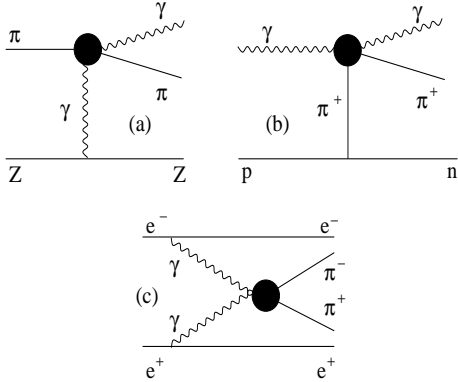


Figure 1: Three pion Compton scattering reactions: (a)  $\pi^-Z \rightarrow \pi^-Z\gamma$ , (b)  $\gamma p \rightarrow \gamma\pi^+n$ , (c)  $e^+e^- \rightarrow e^+e^-\pi^-\pi^+$ .

Electromagnetic studies with virtual photons have the advantage that the energy and three-momentum of the virtual photon can be varied independently. In the pion  $\gamma^*\pi \rightarrow \gamma\pi$  VCS reaction, where the initial state photon is virtual (far from the quasi-real photons of Primakoff scattering) and the final state photon is real, polarizabilities can be measured in the space like region, inaccessible by RCS [8]. We thereby access the so-called electric  $\bar{\alpha}(q^2)$  and magnetic  $\bar{\beta}(q^2)$  generalized polarizabilities of the pion [9], where  $\bar{\alpha}(0)$  and  $\bar{\beta}(0)$  correspond to the RCS  $\bar{\alpha}$  and  $\bar{\beta}$  pion Compton polarizabilities. The  $q^2$ -dependent  $\bar{\alpha}(q^2)$  determines the change  $\Delta F(q^2)$  in the pion charge form factor  $F(q^2)$  in the presence of a strong electric field. The Fourier transform of  $\bar{\alpha}(q^2)$  provides a picture of the local induced pion charge polarization density [10]. Similarly, first experiments [11] and calculation [12] have been carried out for proton VCS via  $ep \rightarrow ep\gamma$ .

We study experimentally the feasibility of extracting the “pion VCS” reaction:

$$\pi^-e \rightarrow \pi^-e\gamma, \quad (1)$$

as a step in developing pion VCS as a new experimental tool for pion polarizability measurements. The data were taken with the Fermilab E781 SELEX spectrometer [13]. We used a 600 GeV/c  $\pi^-$  beam incident on target atomic electrons, detecting the incident  $\pi^-$  and the final state  $\pi^-$ , electron and  $\gamma$ . Theoretical predictions [14, 15] based on chiral perturbation theory are incorporated into a Monte Carlo simulation of the experiment and are compared to the data. With this theory, we calculated the total cross section (as described later) of the Eq. (1) process for a limited kinematic region discussed later [Eq. (6)], using the Monte Carlo integration program VEGAS [16]. The result is  $\sigma(\text{total}) = 34.7 \pm 0.1$  nb. For the kinematic range considered, the integrated cross sections are not sensitive to the polarizabilities. We nonetheless chose this region in order to obtain sufficient statistics for a first study of the reaction.

## 2 VCS kinematics and theoretical differential cross section

We study reaction (1) in terms of the following five independent invariant variables:

$$\begin{aligned} s &= (p_i + k)^2, \\ s_1 &= (k' + q')^2, \quad s_2 = (p_f + q')^2, \\ r^2 &= (p_i - p_f)^2, \quad q^2 = (k' - k)^2. \end{aligned} \quad (2)$$

Here  $p_i$  is the 4-momentum of the incoming pion,  $k$  is the 4-momentum of the target electron, and  $p_f$ ,  $k'$ ,  $q'$  are the 4-momenta of the outgoing pion, electron, and photon, respectively, as shown in Fig. 2.

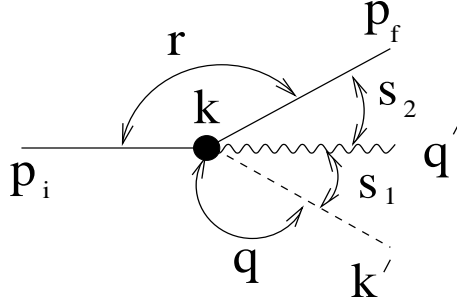


Figure 2: Kinematics of the Eq. (1) reaction in the laboratory frame. The incoming pion beam with 4-momentum  $p_i$  interacts with the target electron with 4-momentum  $k$  and produces the outgoing pion with 4-momentum  $p_f$ ,  $\gamma$  with 4-momentum  $q'$ , and electron with 4-momentum  $k'$ .

The differential cross section of reaction (1) in the convention of Ref. [17] reads as:

$$\begin{aligned} d\sigma &= \frac{m_e^2}{8E_f E_{k'} E_{q'}} \frac{1}{\sqrt{(p_i \cdot k)^2 - M_\pi^2 m_e^2}} \frac{1}{(2\pi)^5} \cdot \\ &|\bar{\mathcal{M}}|^2 \delta^4(p_i + k - p_f - k' - q') d^3 p_f d^3 k' d^3 q'. \end{aligned} \quad (3)$$

The invariant amplitude  $\mathcal{M}$  contains the complete information on the dynamics of the process. The quantity  $|\bar{\mathcal{M}}|^2$  indicates the sum over the final states and the average over the initial spin states. The fourfold differential cross section in terms of independent invariant variables of Eq. (2) involves a kinematical function  $\lambda$  [18] and a Jacobian matrix  $\Delta_4$  defining the phase space of the physical areas, and is given by:

$$\frac{d\sigma}{ds_1 ds_2 dq^2 dr^2} = \frac{1}{(2\pi)^5} \frac{2m_e^2}{\lambda(s, m_e^2, m_\pi^2)} \frac{\pi}{16} \frac{1}{(-\Delta_4)^{1/2}} |\bar{\mathcal{M}}|^2. \quad (4)$$

Since the variable  $s$ , involving the energies of the beam pion and of the target electron, is fixed, differential cross section (4) actually depends on four variables.

In reaction (1), the final photon can be emitted either by the electron or by the pion, as shown in Fig. 3. The first process is described by the Bethe-Heitler (BH) amplitude (Fig. 3a, b), calculable from quantum electro-dynamics.

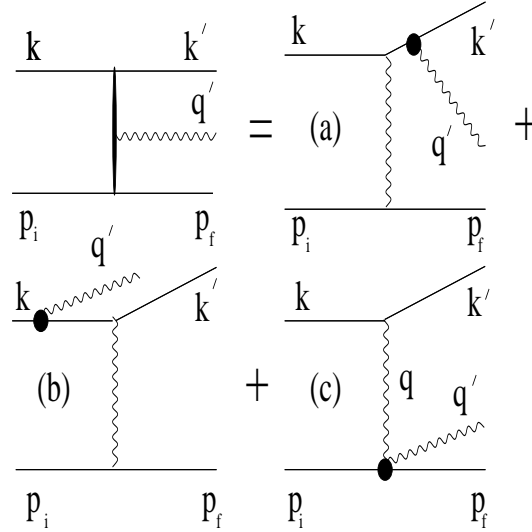


Figure 3: The three Feynman diagrams corresponding to the  $\pi^- e \rightarrow \pi^- e \gamma$ . In the one photon exchange approximation, (a) and (b) correspond to the BH process, while (c) corresponds to the VCS process. Here,  $q$  is the 4-momentum of the virtual photon,  $q = k' - k$ .

The second process is described by the VCS (Fig. 3c) amplitude. Since the source of the final photon emission is indistinguishable, one obtains the following form of the matrix element of reaction (1) [14]:

$$\begin{aligned} |\overline{\mathcal{M}}|^2 &= \frac{1}{2} \sum (\mathcal{M}^{VCS} + \mathcal{M}^{BH})(\mathcal{M}^{VCS*} + \mathcal{M}^{BH*}) \\ &= |\overline{\mathcal{M}^{BH}}|^2 + |\overline{\mathcal{M}^{VCS}}|^2 + |\overline{\mathcal{M}^{VCS}\mathcal{M}^{BH*} + \mathcal{M}^{VCS*}\mathcal{M}^{BH}}|, \end{aligned} \quad (5)$$

where  $\mathcal{M}^{BH}$  and  $\mathcal{M}^{VCS}$  are amplitudes of the BH and VCS processes.

The general features of the four-fold differential cross section can be inferred from Eq. (4) and matrix element calculations. The  $s_1$ -dependence is dominated by the  $(s_1 - m_e^2)^{-1}$  pole of BH, the cross section varies accordingly, and is only slightly modified by the  $s_1$  dependence of the VCS amplitude. The  $s_2$  dependence is dominated by the  $(s_2 - M_\pi^2)^{-1}$  pole of the VCS amplitude with modification of  $s_2$  dependence of the BH amplitude, but in this case the modification is not

as small as in the case of  $s_1$ . The  $r^2$  dependence is determined by the  $r^{-4}$  pole of the BH amplitude, and the  $q^2$  dependence follows the  $q^{-4}$  pole behavior of typical electron scattering. The energy of the outgoing pion is expected to be high while the angle is expected to be small according to the  $r^{-4}$  behavior of the cross section. The energy of the outgoing photon is mainly expected to be low, as follows from the infrared divergence of the BH amplitude. The angular behavior of the outgoing photon is determined by the  $(s_1 - m_e^2)^{-1}$  and  $(s_2 - M_\pi^2)^{-1}$  poles of the BH and VCS amplitudes. The more interesting photons related to the generalized polarizabilities are expected to have higher energies. The behavior of the outgoing electron is completely determined by the  $q^{-4}$  behavior of the cross section.

### 3 Experimental apparatus and trigger

Our data were taken with the Hadron-Electron (HE) scattering trigger [23] of experiment E781/SELEX at Fermilab. SELEX uses a negatively charged beam of 600 GeV/c with full width momentum spread of  $dp/p = \pm 8\%$ , and an opening solid angle of  $0.5 \mu\text{sr}$ . The beam consisted of approximately 50%  $\pi^-$  and 50%  $\Sigma^-$ . SELEX used Copper and Carbon targets, totaling 4.2% of an interaction length, with target electron thicknesses of  $0.676 \text{ barn}^{-1}$  and  $0.645 \text{ barn}^{-1}$ , respectively.

The experiment focused on charm baryon hadroproduction and spectroscopy at large- $x_F$ . The spectrometer hosted several projects which exploit physics with a small number of tracks compared to charm. SELEX had good efficiency for detecting all particles in the final state since the produced particles and decay fragments at large- $x_F$  production are focused in a forward cone in the laboratory frame. Other requirements in the charm program for background suppression include good vertex resolution and particle identification over a large momentum range.

Four dipole magnets divide SELEX into independent spectrometers (Beam, M1, M2 and M3) each dedicated to one special momentum region. Each spectrometer had a combination of tracking detectors. The M1, M2 and M3 spectrometers included electromagnetic calorimeters. The  $\pi - e$  separation for hadron-electron scattering used the M2 particle identification transition radiation detector and also the electromagnetic calorimeter.

The HE scattering trigger was specialized for separation of hadron-electron elastic scattering events. The trigger used information from a charged particle detectors just downstream of the target and, from a hodoscope just downstream of M2, to determine charged particle multiplicity and charge polarity. For the HE requirement, no electromagnetic calorimeter information was included. Therefore, the data collected via this trigger include hadron-electron elastic and inelastic scattering events.

## 4 Monte Carlo Simulation

Monte Carlo simulations were carried out for  $\pi^-$  VCS signal (1) and background event distributions with respect to the four invariants  $s_1$ ,  $s_2$ ,  $q^2$ ,  $r^2$ . We used the SELEX GEANT package GE781 [19]. The Monte Carlo (MC) study was carried out in four steps:

1. A VCS event generator was written to search for the regions of phase space where the data are sensitive to pion structure. Several event generators were made to simulate a variety of expected backgrounds.
2. The event generators were implemented into the simulation package. We studied the resolution, detection efficiency, geometric and trigger acceptances for the signal and background.
3. The offline analysis procedure was developed and tuned to devise software cuts eliminating background while preserving a VCS signal.
4. Finally we estimated the expected number of  $\pi^-$  VCS events.

The VCS event generator is written, based on differential cross section (4), matrix element calculations, and 3-body final state kinematics. The acceptance-rejection method [20] is used for event generation. The VCS cross section increases rapidly when the direction of the outgoing real photon is close to the direction of one of the outgoing charged particles (due to the  $(s_1 - m_e^2)^{-1}$  pole of BH and the  $(s_2 - M_\pi^2)^{-1}$  pole of VCS), or when the energy of the outgoing real photon comes close to zero (due to the infrared divergence of the BH  $((s_1 - m_e^2 - q^2 + r^2)^{-1}$  pole). Therefore, if events are generated in the pole region, then the efficiency of the acceptance-rejection method can be rather low, for the more interesting non-pole regions. In order to generate events at an acceptable rate, the pole regions are eliminated. Invariants are generated in the following regions:

$$\begin{aligned} 1000m_e^2 &\leq s_1 \leq M_\rho^2, \\ 2M_\pi^2 &\leq s_2 \leq M_\rho^2, \\ -0.2 \text{ GeV}^2 &< q^2 < -0.032 \text{ GeV}^2, \\ -0.2 \text{ GeV}^2 &< r^2 < -2m_e E_\gamma(\text{min}) + q^2 + s_1 - m_e^2. \end{aligned} \quad (6)$$

For the photon minimum energy, we choose  $E_\gamma(\text{min}) = 5$  GeV to cut the infrared divergence of BH, and to be above the calorimeter noise. Since the VCS calculation does not explicitly include the  $\rho$  resonance, we choose upper limits of  $M_\rho^2$  for  $s_1$  and  $s_2$ . In Fig. 4, we show the generated distribution of events plotted with respect to the Mandelstam invariants, without correction for any acceptances.

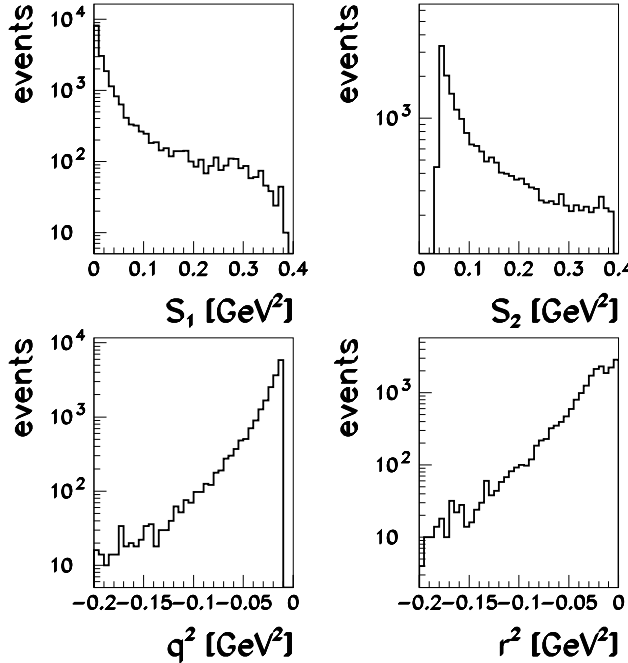


Figure 4: Generated distributions of events plotted with respect to the Mandelstam invariants. The generation was done with 600 GeV/c beam momentum.

Since  $\pi/e$  separation is not 100% efficient, all interactions which produce two negatively charged tracks and a photon in the final state can generate the pattern of the pion VCS; i.e., can create background to the required measurement. For the background simulation, as well as in case of the VCS simulation, we require 5 GeV minimum energy for the photon.

The dominant background process for pion VCS is  $\pi^-e$  elastic scattering followed by final state interactions of the outgoing charged particles, such as Bremsstrahlung. The MC simulation shows that 28% of the original  $\pi^-e$  elastic scattering events generate more than 5 GeV Bremsstrahlung photons somewhere in the SELEX apparatus. We therefore consider the  $s_3$  invariant mass of the outgoing  $\pi^-e$  system:

$$s_3 = (p_f + k')^2. \quad (7)$$

We expect  $s_3 = s$  for elastic scattering, and  $s_3 = s_1 - s_2 + m_e^2 + M_\pi^2$  for VCS.

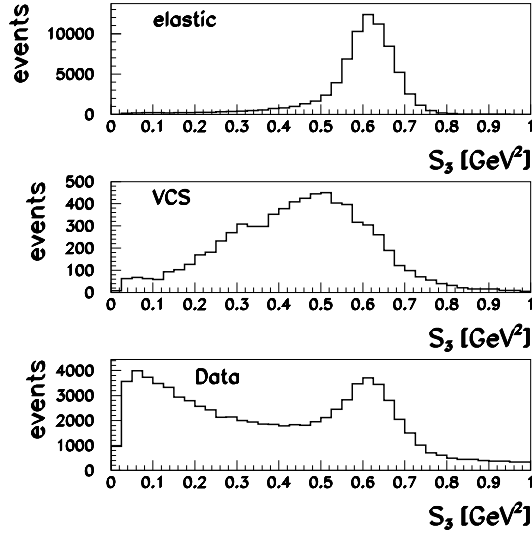


Figure 5: Comparison of simulated  $s_3$  distributions for  $\pi^- e$  elastic scattering (top) and pion VCS (middle) with the data (bottom).

Fig. 5 shows generated and reconstructed elastic and VCS events subjected to the same charged particle track reconstruction and trigger requirements as the data. As seen from Fig. 5, the events at low  $s_3$  do not arise from  $\pi^- e$  elastic or  $\pi^-$  VCS. To describe the events with low  $s_3$ , we simulate backgrounds (with corrections for acceptances) from the interactions:

$$\pi^- e \rightarrow M e, \quad (8)$$

$$\pi^- A(Z) \rightarrow M A(Z), \quad (9)$$

where  $M$  in Eqs. (8) and (9) is an intermediate meson state which can decay via  $\pi^-\pi^0$ ,  $\pi^-\eta$ ,  $\pi^-\omega$ , etc. Considering the threshold energies of reaction (8), only  $\rho$  meson production is allowed at SELEX energies. Fig. 6 shows the simulated  $s_3$  distributions for reactions (8-9), with the same acceptance requirements as in Fig. 5.

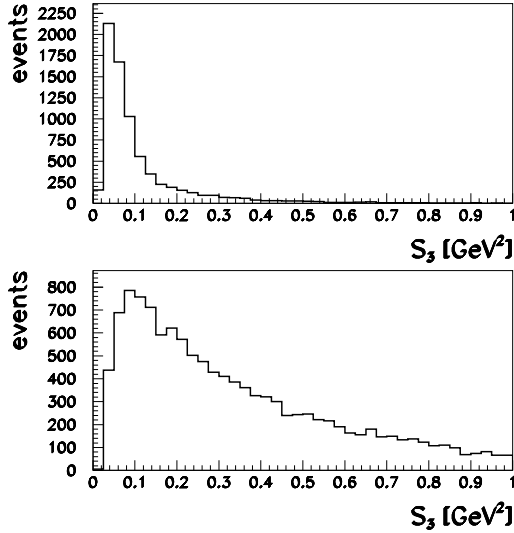


Figure 6: Background via meson production: simulated  $s_3$  distribution for  $\pi^- e \rightarrow \rho e'$  (upper), and for  $\pi^- A(Z) \rightarrow MA(Z)$  (lower), with arbitrary normalization.

SELEX GE781 allows us to estimate the background rate from  $\pi^- e$  elastic scattering. However, it is very difficult to estimate the background rate from all  $\pi^0$  production reactions. Consequently, we seek a set of cuts which remove as “completely” as possible the background from all  $\pi^0$  sources.

Since we measure all outgoing particles, the reaction kinematics are over-determined. Therefore, in the data analysis, a constrained  $\chi^2$  fitting procedure [21] is used. A veto condition is used based on a 2-body final state constrained  $\chi^2$  kinematic fit for reduction of the background from  $\pi^- e$  elastic scattering [22]. A 3-body final state constrained  $\chi^2$  kinematic fit is used for extracting the pion VCS signal.

A final state electron can arise from photon conversion. For this background, the electron is not created at the same vertex as the pion. Consequently, the quality of the 3-track vertex reconstruction should be low. Also, the simulation shows that no VCS outgoing particles hit the upstream photon calorimeter. Therefore, in addition to the constrained kinematic fitting cuts, we use restrictions on the vertex quality and on the total energy deposit in the upstream photon calorimeter to suppress backgrounds.

An additional way to reduce the background from  $\pi^- e$  elastic scattering is to use the  $\gamma e$  invariant mass  $s_1$  and the  $\Theta_{s_1}$  angle (angle between  $p_i$  and  $(q' + k')$ ; see Fig. 2). The simulation shows that if the final photon is emitted via electron bremsstrahlung, the value of  $s_1$  should be low. On the other hand if the photon

and electron are produced via  $\pi^0$ ,  $\eta$ , or  $\omega$  meson,  $s_1$  will “remember” the mass of the parent particle. Holding the value of the  $s_1$  invariant to be between the squared mass of  $\pi^0$  and  $\eta$  mesons cuts the background from the electron bremsstrahlung and from reactions (9). Fig. 7 shows the distributions of VCS and background simulations. It is seen that the region with higher  $\sqrt{s_1}$  and lower  $\Theta_{s_1}$  are mostly populated with pion VCS.

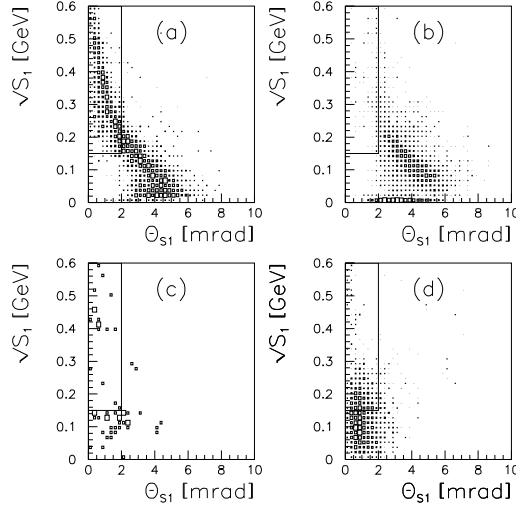


Figure 7:  $\sqrt{s_1}$ ,  $\Theta_{s_1}$  correlation for (a) VCS, (b)  $\pi^-e$  elastic scattering, (c) intermediate meson, and (d)  $\rho$  meson production. Only events inside the  $\Theta_{s_1}$ - $\sqrt{s_1}$  region indicated by the box were accepted for the further analysis.

Another possibility to reduce the background from interactions (8-9) is to cut on the invariant  $M$ , defined as:

$$M = \sqrt{(P_\pi + P_e - P_{e'})^2}. \quad (10)$$

For elastic events  $M = M_\pi$ , for VCS  $M = \sqrt{s_2}$ , for  $\rho$  production  $M = M_\rho$  (see Fig. 8).

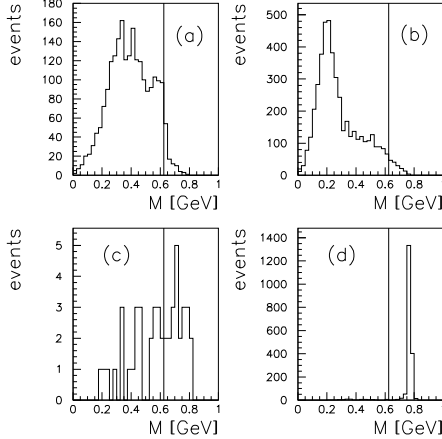


Figure 8: Generated distribution of the  $M$  invariant for: (a) VCS, (b) elastic scattering, (c) meson production reactions (9), and (d)  $\rho$  production reaction (8). The vertical lines show the 0.625 GeV  $M$ -cut position.

The set of the final cuts follows:

- **1**, fulfillment of the pion VCS pattern with: identified electron;  $E_\gamma \geq 5$  GeV for photons observed at laboratory angles less than 20 mrad in the downstream electromagnetic calorimeters; no additional tracks and vertices; the total energy deposit is less than 1 GeV in the upstream electromagnetic calorimeter, covering detection angles greater than 30 mrad.
- **2**, Eq. (6) ranges for the invariants, with  $s_1(\min) = 0.0225$  GeV $^2$ .
- **3**,  $\chi^2_{elastic} > 20$ , following a constrained fit procedure [21, 22].
- **4**,  $\chi^2_{VCS} \leq 5$ , following a constrained fit procedure [21, 14].
- **5**,  $\Theta_{s_1} < 2$  mrad,  $M \leq 0.625$  GeV.

To estimate the number of expected VCS events, as well as the yields of other  $\pi^-e$  elastic or inelastic scattering events, we use:

$$N_{\pi e} = N_\pi \cdot \sigma \cdot N_T \cdot \epsilon_{ex} \cdot \epsilon_r. \quad (11)$$

Here  $N_{\pi e}$  is the number of events observed for a particular  $\pi e$  reaction,  $N_\pi$  is the number of incident beam pions ( $\sim 4.4 \cdot 10^{10}$  as measured by beam scalers and including particle identification),  $\sigma$  is the cross section for the particular reaction,

$\epsilon_r$  is the offline reconstruction efficiency (36.6% for elastic, 2.65% for VCS) of the studied process, and  $N_T$  is the target electron density. Since not all experimental properties are implemented in GEANT, an additional efficiency factor  $\epsilon_{ex}$  is included in Eq. 11. This efficiency factor is common to  $\pi e$  elastic and pion VCS reactions. The value  $\epsilon_{ex}$  is calculated by comparison of the actual number of observed  $\pi e$  elastic scattering events to the expected number of events. The common efficiency arises since these two reactions have practically the same  $q^2$  dependence;  $q^2$  being the only kinematical parameter relevant for the trigger and first order data reduction procedure. We calculate the experimental efficiency  $\epsilon_{ex}$  (13.4%) from  $\pi e$  elastic scattering, as described in Ref. [14]. For extraction of the reference  $\pi e$  elastic scattering events, we employ the cuts of the SELEX  $\pi e$  elastic scattering analysis [22]. The cuts described above, considering the studied sources of background, improve the signal/noise ratio from less than 1/400 to more than 361/1. For these estimates, we used the following cross sections:  $\sigma_{VCS} = 34.7 \text{ nbarn}$  and  $\sigma_{elastic} = 4.27 \mu\text{barn}$  for  $\pi e$  scattering;  $\sigma_{Primakoff}(C \text{ target}) = 0.025 \text{ mbarn}$  and  $\sigma_{Primakoff}(Cu \text{ target}) = 0.83 \text{ mbarn}$  for the  $Z^2$ -dependent Primakoff scattering. Based on the calculated pion VCS cross section, we expect  $\sim 8$  events in the  $\pi^-$  data sample.

The effect of the above enumerated cuts on the VCS signal, and on the backgrounds coming from  $\pi e$  elastic scattering and Primakoff meson production, are listed in Table 2. The results are based on the estimated relative cross section for these three processes [14]. The cuts are very effective in removing backgrounds while retaining signal events.

Cuts	VCS	Elastic	Meson production
1	29.8	32.1	0.24
2	9.97	9.21	0.03
3	8.89	0.03	0.03
4	3.58	0.003	0.004
5	2.56	< 0.003	< 0.004

Table 2: Percentages of the remaining events after using the cuts for the MC simulated  $\pi$  VCS and background events.

## 5 Data Analysis

In the first stage analysis, events containing one identified electron are selected. For these events, particle trajectories are checked if they form a vertex inside the target material. An event is accepted if it contains exactly three tracks, including the beam particle and an electron candidate, and forms one vertex in the target.

On the accepted data set, we applied the system of the cuts discussed above. The working statistics with these cuts on the data are given in Table 3.

cuts	% of remain events
1	31.1
2	1.2
3	0.88
4	0.05
5	0.01

Table 3: Percentages of events remaining after using the cuts.

Finally 9 events (with a statistical uncertainty  $\pm 3$ ) were accepted as pion VCS. The corresponding  $\pi$  VCS experimental cross section based on Eq. (11) under the assumption that the background has been completely eliminated is  $\sigma = 38.8 \pm 13$  nb, in agreement with the theoretical expectation  $\sigma = 34.7$  nb. The error given is only statistical, and does not include possible systematic uncertainties in the efficiency product  $\epsilon_{ex} \cdot \epsilon_r$  in Eq. (11).

The comparisons of reconstructed (data) and generated (theory) event distributions, normalized to unit area are shown in Fig. 9 with respect to the four invariants  $s_1$ ,  $s_2$ ,  $q^2$  and  $r^2$  of Eq. (2), shown with binning that roughly matches the experimental resolutions.

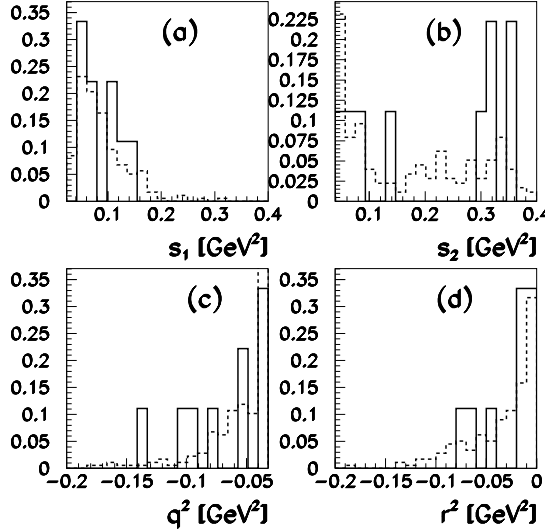


Figure 9: Comparison of data and theory normalized distributions with respect to: (a)  $s_1$ , (b)  $s_2$ , (c)  $q^2$ , and (d)  $r^2$ . The solid line corresponds to data, the dashed line corresponds to simulations with  $\bar{\alpha} = 2.7$ . The simulation with  $\bar{\alpha} = 6.8$  gives practically the same result.

To check whether the data and theory (MC) distributions are consistent with each other, we use the K-S test of Kolmogorov and Smirnov [25]. The K-S test is based on normalized cumulative distribution functions (CDF). We use the K-S  $D$  statistic, as a measure of the overall difference between the two CDFs. It is defined as the maximum value of the absolute difference between two CDFs. The significance level for a value  $D$  (as a disproof of the null hypothesis that the distributions are the same) is given by the probability  $P(D)$  [25]. A high value of  $P(D)$  means that the data and theory CDF are consistent with one another.

Following the K-S procedure, we calculate the normalized cumulative distributions of data and theory, corresponding to Figs. 9a-d. The K-S  $D$  statistic, and the K-S probabilities for consistency of theory/data distributions, are given in Table 4 and Fig. 10.

variable	$D$	$P(D)$
$s_1$	0.13	0.99
$s_2$	0.33	0.18
$q^2$	0.24	0.54
$r^2$	0.19	0.81

Table 4: Value of K-S  $D$  statistic, and probabilities  $P$ , for comparison of data with theory for  $\bar{\alpha} = 2.7$ . The comparison of data with theory for  $\bar{\alpha} = 6.8$  gives practically the same result.

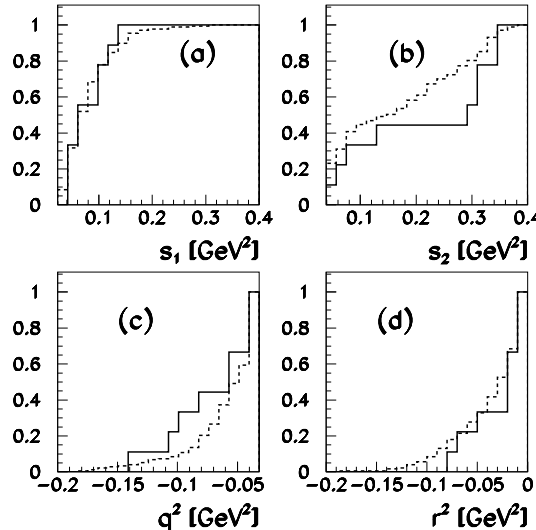


Figure 10: Normalized cumulative distributions for data and theory versus: (a)  $s_1$ , (b)  $s_2$ , (c)  $q^2$ , and (d)  $r^2$  invariants. The solid line corresponds to data, the dashed line corresponds to MC theory simulations with  $\bar{\alpha} = 2.7$ . The simulation with  $\bar{\alpha} = 6.8$  gives practically the same result

The experimental and theoretical CDFs for  $s_1$  and  $r^2$  look similar. For  $s_2$  and  $q^2$ , some regions of  $q^2$  ( $s_2$ ) have the experimental CDFs larger (smaller) than the theoretical CDFs. The values of  $P(D)$  (see Table 4) are sufficiently high for all four CDF's, as expected if the experimental data are consistent with theory. In addition, the prediction of a total of 8 events is in agreement with the observed  $9 \pm 3$  data events. This further supports the conclusion from the K-S test that we observe pion VCS events.

From the limited statistics and sensitivity of this first pion VCS experiment, we cannot determine the  $\bar{\alpha}$  polarizability value, nor can we determine which value of  $\bar{\alpha}$  is preferred. In a future experiment, the sensitivity to pion polarizability may be increased [14] by achieving a data set in which the final  $\gamma$  ( $\pi$ ) has higher (lower) energies. However, such data correspond to a lower cross section, and therefore require a high luminosity experiment.

## 6 Conclusions

The pion Virtual Compton Scattering via the reaction  $\pi e \rightarrow \pi' e' \gamma$  is observed. We developed and implemented a simulation with a VCS event generator. We defined cuts that allow background reduction and VCS signal extraction. The measured number of reconstructed pion VCS events, and their distributions with respect to the Mandelstam invariants, are in reasonable agreement with theoretical expectations. The corresponding  $\pi$  VCS experimental cross section is  $\sigma = 38.8 \pm 13$  nb, in agreement with the theoretical expectation  $\sigma = 34.7$  nb.

## 7 Acknowledgments

The authors are indebted to the staffs of Fermi National Accelerator Laboratory, the Max-Planck-Institut für Kernphysik, Carnegie Mellon University, Petersburg Nuclear Physics Institute and Tel Aviv University for invaluable technical support. We thank Drs. C. Unkmeir and S. Scherer for the VCS matrix element calculation.

This project was supported in part by Bundesministerium für Bildung, Wissenschaft, Forschung und Technologie, Consejo Nacional de Ciencia y Tecnología (CONACyT), Conselho Nacional de Desenvolvimento Científico e Tecnológico, Fondo de Apoyo a la Investigación (UASLP), Fundação de Amparo à Pesquisa do Estado de São Paulo (FAPESP), the Israel Science Foundation founded by the Israel Academy of Sciences and Humanities, Istituto Nazionale de Fisica Nucleare (INFN), the International Science Foundation (ISF), the National Science Foundation (Phy #9602178), NATO (grant CR6.941058-1360/94), the Russian Academy of Science, the Russian Ministry of Science and Technology, the Turkish Scientific and Technological Research Board (TÜBITAK), the U.S. Department of Energy (DOE grant DE-FG02-91ER40664 and DOE contract number DE-AC02-76CHO3000), and the U.S.-Israel Binational Science Foundation (BSF).

## References

- [1] J. Portales, M. R. Pennington, hep-ph/9407295,  
D. Morgan and M. R. Pennington, Phys. Lett. **B272** (1991) 134.

- [2] D. Babusci et al., Phys. Lett. **B277** (1992) 158.
- [3] B. R. Holstein, Comments Nucl. Part. Phys. **19** (1990) 221.
- [4] A. Klein, Phys. Rev. **99** (1955) 988;  
 A. M. Baldin, Nucl. Phys. **18** (1960) 310;  
 V. A. Petrun'kin, Sov. JETF. **40** (1961) 1148.
- [5] Yu. M. Antipov et al., Phys. Let. **B121** (1983) 445;  
 Yu. M. Antipov et al., Z.Phys.C **26** (1985) 495.
- [6] T. A. Aibergenov at al., Czech. J. Phys. **36** (1986) 948.
- [7] J. Boyer et al., Phys. Rev. **D42** (1990) 1350.
- [8] S. Scherer, hep-ph/9807562; nucl-th/9901056; Czech. J. Phys. **49** (1999) 1307.
- [9] C. Unkmeir et al., Phys. Rev. **D61** (2000) 034002.
- [10] A. I. Lvov et al., Phys. Rev. **C64** (2001) 015203.
- [11] S. Kerhoas et al., Nucl. Phys. **A666-667** (2000) 44,  
 J. Roche et al., Phys. Rev. Lett. **85** (2000) 708.
- [12] B. Pasquini et al., Phys. Rev. **C63** (2001) 025205; nucl-th/0105074;  
 and references therein.
- [13] J. Russ et al., A proposal to construct SELEX, Proposal PE781, Fermilab,  
 1987, <http://fn781a.fnal.gov/>.
- [14] C. Unkmeir et al., hep-ph/0107020, Phys. Rev. **C** (accepted for publication).  
 A. Ocherashvili, Pion Virtual Compton Scattering, Ph.D. thesis, Sept. 2000,  
 Tel Aviv University, <http://muon.tau.ac.il/~aharon/phd.html>.
- [15] S. Scherer, hep-ph/9807562,  
 C. Unkmeir et al., hep-ph/9904442,  
 C. Unkmeir, Pion Polarizabilities in the reaction of radiative pion photoproduction on the proton, Ph.D. thesis, Johannes Gutenberg University, Mainz,  
 Sept. 2000,  
 T. Fuchs et al., hep-ph/0010218.
- [16] G.P. Lepage, J. Comp. Phys. **27** (1978) 192.
- [17] J. D. Bjorken, S. D. Drell, Relativistic Quantum Mechanics, McGraw-Hill,  
 New York, 1964.
- [18] E. Byckling K. Kajantie, Particle Kinematics, Three Particle Final State,  
 JohnWiley & Son Ltd, 1973.

- [19] G. Davidenko et al., GE781: a Monte Carlo package for fixed target experiments, in: R. Shellard and T. D. Nguyen, eds., *Proceedings of the International Conference on Computing in High Energy Physics'95* (World Scientific, Singapore, 1996) p.832,  
 G. Dirkes, H. Krüger, N. P. Kuropatkin, J. Simon, data and GE781 comparison for elastic scattering physics, MPI Heidelberg, 1999 (Unpublished),  
 V. Steiner, GE781 code development for Hadron Electron topics, SELEX Collaboration Meeting Presentations and Private communications,  
 I. Giller, Measurement of the pion charge radius, M.Sc. thesis, Tel Aviv University, 1999,  
 I. Eschrich et al., hep-ex/0106053.
- [20] C. Caso et al. (PDG), Eur. Phys. J. **C3** (1998) 1-794.
- [21] S. Brandt, Data Analysis: Statistical and Computational Methods for Scientists and Engineers, Springer Verlag, 1998.
- [22] J. Simon, Messung des elektromagnetischen Ladungsradius des sigma- bei 600 GeV/c (in German), Ph.D. thesis, MPI Heidelberg, 2000,  
 G. Dirkes, Messung der elektromagnetischen Formfaktoren von Pionen im SELEX Experiment (in German), M.Sc. thesis, MPI Heidelberg, 1999.
- [23] K. Vorwalter, Determination of the pion charged radius with a silicon microstrip detector system, Ph.D. thesis, MPI f. Kernphysik / Univ. Heidelberg, 1998,  
 H. Krüger, Untersuchung der elastischen Hadron-Elektron-Streuung bei 540 GeV/c zur Messung des elektromagnetischen Ladungsradius des Protons (in German), Ph.D. thesis, MPI Heidelberg, 1999.
- [24] P. Mathew, Construction and evaluation of a high resolution silicon microstrip tracking detector, and utilization to determine interaction vertices, Ph.D. thesis, Carnegie Mellon University, 1997,  
 J. L. Langland, Hyperon and anti-hyperon production in  $p - Cu$  interactions. Ph.D. thesis, University of Iowa, 1996. UMI-96-03058,  
 J. L. Langland, Hyperon beam flux parameterization for E781 based on E497 data, H-note 693, SELEX Internal Report, 1994.
- [25] Numerical Recipes in FORTRAN: The Art of Scientific Computing, W. H. Press et al., University of Cambridge, 1992.